ACCEPTED BY THE ASTROPHYSICAL JOURNAL 2003 JULY 7
Preprint typeset using LaTeX style emulateapj v. 11/12/01

HIGH-RESOLUTION CONTINUUM IMAGING AT 1.3 AND 0.7 CM OF THE W3 IRS 5 REGION

T. L. WILSON[1], D. A. BOBOLTZ[2], R. A. GAUME[2], S. T. MEGEATH[3]
Accepted by the Astrophysical Journal 2003 July 7

ABSTRACT

High-resolution images of the hypercompact HII regions (HCHII) in W3 IRS 5 taken with the Very Large Array (VLA) at 1.3 and 0.7 cm are presented. Four HCHII regions were detected with sufficient signal-to-noise ratios to allow the determination of relevant parameters such as source position, size and flux density. The sources are slightly extended in our $\sim$0.2″ beams; the deconvolved radii are less than 240 AU. A comparison of our data with VLA images taken at epoch 1989.1 shows proper motions for sources IRS 5a and IRS 5f. Between 1989.1 and 2002.5, we find a proper motion of 210 mas at a position angle of 12° for IRS 5f and a proper motion of 190 mas at a position angle of 50° for IRS 5a. At the assumed distance to W3 IRS 5, 1.83$\pm$0.14 kpc, these offsets translate to proper motions of $\sim$135 km s^{-1} and $\sim$122 km s^{-1} respectively. These sources are either shock ionized gas in an outflow or ionized gas ejected from high mass stars. We find no change in the positions of IRS 5d1/d2 and IRS 5b; and we show through a comparison with archival NICMOS 2.2 μm images that these two radio sources coincide with the infrared double constituting W3 IRS 5. These sources contain B or perhaps O stars. The flux densities of the four sources have changed compared to the epoch 1989.1 results. In our epoch 2002.5 data, *none* of the spectral indicies obtained from flux densities at 1.3 and 0.7 cm are consistent with optically thin free-free emission; IRS 5d1/d2 shows the largest increase in flux density from 1.3 cm to 0.7 cm. This may be an indication of free-free optical depth within an ionized wind, a photoevaporating disk, or an accretion flow. It is less likely that this increase is caused by dust emission at 0.7 cm.

Subject headings: H II regions–ISM:individual(W3)–radio continuum:ISM–stars: formation

1. INTRODUCTION

W3 is a high-mass star formation region located in the Perseus arm at a distance of 1.83$\pm$0.14 kpc as determined from H_2O maser proper motions (Imai et al. 2000). W3 contains several sites of star formation, the most active of which is W3 Main, which contains at least 10 young high mass stars and protostars within a region spanning only a few parsecs. The molecular gas in W3 Main is distributed into two distinct molecular clumps (Tieftrunk et al. 1995). The eastern clump appears to be the more active of the two clumps and is associated with two bright, extended HII regions. The more evolved, shell-like HII region, W3A, lies to the east of the more compact HII region W3B (see Tieftrunk et al. 1997, hereafter TGC97).

Located between W3A and W3B is the luminous infrared source W3 IRS 5. This source was first discovered by Wynn-Williams, Becklin & Neugebauer (1972). Because of the lack of radio continuum emission toward IRS 5, Wynn-Williams, Becklin & Neugebauer (1972) suggested that IRS 5 was in a protostellar phase. Subsequent observations at infrared and submillimeter wavelengths showed a steeply rising spectral energy distribution from 2 to 50 μm with a peak at 100 μm and a total luminosity greater than 10^5 $L_\odot$ (Campbell et al. 1995). Infrared slit-scan and speckle measurements resolved IRS 5 into a double source with a separation of 1″ (Neugebauer, Becklin & Matthews 1982; Howell, McCarthy & Low 1981). Wide-field infrared imaging has detected a dense cluster of at least 80 low mass stars surrounding W3 IRS 5; these stars are distributed over a region 40″ (0.5 pc) in diameter (see Megeath et al. 1996). Chandra observations have detected a X-ray source toward W3 IRS 5, making IRS 5 a rare system of massive young stellar objects that can be studied from X-ray to radio wavelengths (Hofner et al. 2002).

Molecular line observations have produced ample evidence that IRS 5 is the source of at least one molecular outflow. CO observations show a bipolar outflow centered on IRS 5 with an axis oriented in northeast–southwest direction and a position angle of $\sim$38^o (Claussen et al. 1984; Mitchell et al. 1991). Proper motion measurements of a cluster of H_2O masers surrounding W3 IRS 5 show an overall motion away from IRS 5, which when combined with radial measurements, can be modeled as two distinct outflows aligned roughly north–south (Imai et al. 2000; Imai, Deguchi & Sasao 2002). Infrared spectroscopy of CO fundamental absorption features toward IRS 5 revealed three blueshifted components suggestive of multiple outbursts (Mitchell et al. 1991). From their 0.87 mm line survey, Helmich & van Dishoeck (1997) found that W3 IRS 5 is a region in which shock chemistry is present.

Relatively weak radio emission toward IRS 5 was first detected by Colley (1980), who named the radio source W3 M. More recent VLA observations have resolved W3 M into a cluster of seven distinct centimeter radio sources with fluxes around $\sim$ 1 mJy, distributed over a region 3″ (5000 AU) in diameter (TGC97, (Claussen et al. 1994, hereafter CG94)).

The nature of the radio source remains enigmatic. These are examples of a growing number of H II regions with sizes less than few 10^3 AU, called hypercompact HII regions (HCHII) (Gaume et al. 1995). An outstanding question is the relationship between the two infrared sources and the seven sources detected in the radio. One possibility is that most of the radio sources are too deeply embedded to be detected in the infrared. An alternative is that the radio sources trace shock ionized regions in the W3 IRS 5 outflow that are not luminous in the infrared. To further investigate the nature of the radio sources,

[1] Max-Planck-Institut für Radioastronomie, Postfach 2024, D-53010 Bonn, Germany
[2] U. S. Naval Observatory, 3450 Massachusetts Ave., NW, Washington, DC 20392-5420
[3] Harvard-Smithsonian Center for Astrophysics, 60 Garden Street, Cambridge, MA 02138

and to better understand the relationship between the radio and infrared sources, we have obtained an additional epoch of VLA measurements of IRS 5. The first detailed images of the IRS 5 region were produced with the VLA A-array at 2 cm in 1989 January (CG94) multi-frequency, multi-array, VLA study carried out by TGC97 with observations at 6, 2, and 1.3 cm from 1989 January to September. The shortest wavelength observed by both CG94 and TGC97 was 1.3 cm. The HCHII regions may be optically thick at 1.3 cm, therefore measurements at 0.7 cm, where dust emission should not contribute to the free–free emission, are of great value in determining parameters such as emission measure, electron density and the mass of ionized gas for these sources.

We have measured W3 IRS 5 with the VLA B-configuration at both 1.3 and 0.7 cm. If the HCHII regions are ionized by embedded stars, these observations allow us to estimate the Lyman continuum photon flux and to classify the exciting stars. In addition, we can compare our results with those of CG94, to look for variations in source position and flux density over time that may be indicative of a shock origin for the radio sources. Additional comparisons are made with archival near IR data taken with the NICMOS camera on board the Hubble Space Telescope.

2. OBSERVATIONS AND REDUCTION

We observed W3 IRS 5 using the VLA, which is maintained and operated by the National Radio Astronomy Observatory (NRAO)[4]. The B-configuration observations occurred over an 8 hr period beginning 2002 July 11 at 23:00 LST. High-frequency continuum measurements at 1.3 and 0.7 cm were conducted in dual-polarization mode using four intermediate frequencies (IFs), two in left circular polarization and two in right circular polarization. Two adjacent 50-MHz bands were recorded for a total spanned bandwidth of 100 MHz centered on 22485.1 MHz for the 1.3 cm measurements and 43364.9 MHz for the 0.7 cm measurements. In order to reduce the effects of atmospheric phase fluctuations, we used the technique of *fast-switching* (Carilli & Holdaway 1997) between the target, W3 IRS 5, and a phase calibrator, 0228+673, that is 5.3^o away from W3 IRS 5. We observed with a fast-switched cycle time of 110 s, with 80 s spent on the target and 30 s on the calibrator. Cycles were repeated for 30 minutes at 0.7 cm followed by 30 minutes at 1.3 cm. A reference pointing scan at 3.5 cm on 0228+673 was performed prior to the start of each 0.7 cm 30-minute scan. Finally, two scans were recorded each at 1.3 and 0.7 cm on the calibrator source 0713+438, which is recommended by the NRAO for use in determining the absolute flux density calibration at high frequencies and is regularly monitored by the VLA at both 1.3 and 0.7 cm.

Data were reduced using the standard routines within the Astronomical Image Processing System (AIPS). The absolute flux density scale was established using fluxes for 0713+438 determined by the VLA in B-configuration on 2002 June 24, roughly two weeks prior to our observations. These flux densities were 0.506 ± 0.002 Jy at 1.3 cm and 0.263 ± 0.003 Jy at 0.7 cm. Target source phases were calibrated by interpolating the phases from the fast-switched phase calibrator source 0228+673. From the amplitude and phase calibrated data, a number of images of both the large scale structure of the W3 region and the compact sources in the W3 IRS 5 region were produced. Figures 1 and 2 show the compact radio emission toward W3 IRS 5 at 1.3 cm and 0.7 cm respectively. For purposes of comparison both images were produced using a circular $0.2''$ beam. Also plotted in Figures 1 and 2 are crosses which represent positions of features observed by CG94 and TGC97 along with the corresponding letter designations. Our contour maps show four distinct regions of emission near the CG94 positions for sources IRS 5a, b, d1/d2 and e/f.

In order to extract relevant parameters such as source positions and flux densities, two-dimensional Gaussian functions were fitted to the four features visible in Figures 1 and 2 using the AIPS task JMFIT. In addition, we determined upper limits on the flux densities corresponding to CG94/TGC97 sources IRS 5c, d1, e, and g. We accomplished this by integrating image flux densities over a $0.2'' \times 0.2''$ box centered on the CG94/TGC97 positions using the AIPS task IMEAN. This task was complicated by blending in the case of feature IRS 5d1 (discussed below). The results from the fits to the images analysis and the interpretation are discussed in the next section.

3. RESULTS AND DISCUSSION

3.1. *Proper Motions*

In Table 1 we give the Gaussian fit results for the four sources visible in our 1.3 cm and 0.7 cm data. The most intense source at both wavelengths is source IRS 5d2. Since our images do not completely resolve CG94 sources d1 and d2, it is possible that the position and flux density for d2 in Table 1 suffer from some blending with the weaker source d1. In the following we refer to this as d1/d2. Examination of Figures 1 and 2 shows that the most northern source in our images appears to be equidistant from the CG94 positions for IRS 5e and f. Because CG94 found that IRS 5f had twice the flux density of IRS 5e at 2 cm, we believe it more likely that the stronger of the two sources brightened while the weaker source is no longer seen. We therefore identify this peak with CG94 source IRS 5f in subsequent discussion.

In Figures 1 and 2 there appears to be a slight ($\sim0.02''$) shift in $\alpha\cos(\delta)$ between two of the peaks in our images and the CG94 sources d1/d2 and b. Since we have no absolute reference with which to register the two sets of positions, we have chosen to compare relative angular distances between features, which we term arclengths. For example, the distance between source d1/d2 and source f is arclength f-d1/d2. In Table 2 we compare the arclengths derived from our 1.3 cm and 0.7 cm data with those computed from the CG94 data at 2 cm. Examination of the table shows that the arclength d1/d2–b remained nearly unchanged to within 19 milli-arcseconds (mas) or less. However, f-d1/d2 and f–b both show offsets greater than 200 mas at comparable positions angles. These differences imply that sources IRS 5d1/d2 and b were stationary between the epoch of our observations and that of CG94, and that source IRS 5f is moving away from IRS 5b and d1/d2 in a direction $\sim12^\circ$ east of north. Over the time period between the two epochs the $\sim$210 mas offset translates to a rate of ~15.6 mas yr^{-1}. The estimated uncertainty in the arclength differences is 10%. At the assumed distance to W3 IRS 5, the proper motion is 135 km s^{-1}. The angular separation between IRS 5f and d1/d2 in our 1.3 cm image is $0.56''$. The proper motion of IRS 5f is in a direction approximately away from IRS 5d1/d2. If IRS 5f originated from IRS 5d1/d2, and the velocity of IRS 5f remained constant, the travel time from IRS 5d1/d2 to the Epoch 2002.5 position of IRS 5f is 36 years.

[4] The National Radio Astronomy Observatory is a facility of the National Science Foundation operated under cooperative agreement by Associated Universities, Inc.

For source IRS 5a the position uncertainties are greater in Table 1 because of the lower signal-to-noise ratios for the peaks, especially at 1.3 cm. Nevertheless, the measured position of IRS 5a using the 1.3 cm data and that using the 0.7 cm data are in good agreement, as seen in Table 2. Both show a proper motion of IRS 5a relative to stationary IRS 5b and IRS 5d1/d2. Offsets between our 0.7 cm positions and those of CG94 are $\sim$190 mas at a position angle of 50° E of N. This offset translates to a motion of $\sim$14.1 mas yr^{-1} or 122 km s^{-1} at the assumed distance to W3 IRS 5. The magnitude of this velocity is similar to that of component IRS 5f.

Since there may be additional motion along the line of sight, the measured velocities of IRS 5f and IRS 5a are lower limits. Given the large magnitude of the velocities, it is unlikely that IRS 5f and IRS 5a contain stars. However, such velocities are often found in outflows. Thus we propose that these components formed in outflows originating in the W3 IRS 5 system. As surveyed in the Introduction, there is ample evidence that W3 IRS 5 is driving an outflow. The evidence includes the presence of a CO outflow and an expanding cluster of H_2O masers (Imai et al. (2000)). Imai et al. (2000) studied the proper motions of the H_2O masers toward the IRS 5 region and determined proper motions for 108 maser features some of which are near the continuum sources IRS 5a, b, c and e. They concluded that these motions are caused by two distinct outflows aligned north–south with origins approximately 700 mas south of IRS 5d1/d2 and 300 mas north of IRS 5a. Since the motion of source IRS 5f is in agreement with this north–south direction, this lends support to our identification of our northern source with CG94 source IRS 5f. The alternative would be motion of source IRS 5e in a direction counter to the outflow directions suggested by the maser proper motions. We consider this scenario unlikely. Near source IRS 5a, there is a group of H_2O masers with proper motions directed to the west, although the speeds implied by the H_2O maser proper motions are $\sim$20% of the speed inferred for IRS 5a. Our data show that source IRS 5a is moving in nearly the opposite direction from these nearby masers with a proper motion $\sim$50° east of north. This position angle is actually closer to the CO outflow direction of 38° observed by Mitchell et al. (1991) than to the two suggested north–south maser outflows. We show a superposition of the locations of IRS 5d1/d2, b, a and f, together with the H_2O masers and near IR sources in Fig. 3.

It is interesting that the two continuum sources for which we observe proper motions have relatively few H_2O masers in their vicinity and that these few masers have motions that are peculiar to the general north–south flow. In the case of source IRS 5f, the closest maser is a single feature near CG94 component IRS 5e with a motion toward the SE. Thus we find an indication of an anti-correlation of continuum source proper motions and presence of water masers. Imai et al. (2000) suggest that the maser clusters apparent in W3 IRS 5 (see Fig. 3) are formed in a compressed shell of turbulent post-shock gas swept up by outflows. We find it plausible that the continuum sources IRS 5a and f are part of supersonic outflows sweeping up the ambient gas.

3.2. *Source Flux Densities*

In Table 3 we compare integrated source flux densities from our data and that of CG94 and TGC97. For sources IRS 5a, b, d2, and f, our reported flux densities are the results of the Gaussian fits to the peaks. For sources IRS 5c, d1, e and g we used the AIPS task IMEAN as discussed in Section 2. For sources IRS 5c, e, and g the IMEAN results were below the 3σ rms noise level in the 1.3 and 0.7 cm images and thus represent upper limits on the flux densities. As mentioned in Section 2, the IMEAN result for source IRS 5d1 should be viewed as an upper limit since there is blending from source IRS 5d2. Also, the flux density of d2 may contain a contribution from d1. The values in Table 3 longward of 2 cm are taken from TGC97. For IRS 5g, all of the flux densities are compiled by TGC97. CG94 have tabulated flux densities for individual sources at 2 cm but their 1.3 cm images did not resolve all features. Instead, they cataloged 1.3 cm flux densities for three sources designated a+b, c+d1/d2 and e+f. Summed flux densities for these sources are also reported in Table 3. At 1.3 cm, we make comparisons on a source-by-source basis with the data of TGC97. Our flux densities for sources IRS 5a, b, d2 and f are a factor of 2–4 larger than those of TGC97, while the flux density of IRS 5d1 is approximately equal to or lower than that of TGC97. For sources IRS 5e and g, which we did not detect, our 3σ upper limits are 0.6 and 0.8 times the values determined by TGC97.

It is unlikely that random errors are the cause of the differences, given the signal to noise ratios. Recent improvements in VLA instrumentation (i.e. K-band receiver upgrades) and data taking techniques (i.e. fast-switching) provide greatly improved sensitivity and reduced atmospheric decorrelation for data taken at shorter wavelengths. Thus it is possible that for IRS 5a, b, d2 and f, one might expect our measured flux densities to be higher, even if the sources were not varying over time. However, sources IRS 5e and g, which were observed by TGC97 but are undetected in our 2002 observations, provide evidence for time variability of the continuum sources in the W3 IRS 5 region.

At longer wavelengths, the TGC97 data show that for sources IRS 5d1, d2, e and f the 6 cm flux densities are greater, on average by a factor of 2, than those at 2 cm. This may be an indication that synchrotron emission contributes to the radio emission at longer wavelengths. Synchrotron emission has been found toward the Turner-Welch source in the W3(OH) star forming region (Reid et al. (1995)). Presumably high magnetic fields enhance this emission. (Wilner, Reid & Menten 1999) have carried out detailed, high resolution measurements of the TW object in the W3(OH) region at 8.4 GHz with the VLA. There are some similarites with IRS 5, since the TW source is driving an H_2O maser outflow and has thermal dust emission. Felli et al. (1993) observed a population of HCHII regions in the Orion Nebula with non-thermal spectral indicies and variable flux densities. They speculated that these changes were caused by photospheric phenomena. It is possible that we are measuring a similar type of phenomenon, although the flux densities of the IRS 5 sources are about 20 times larger than those in Orion, and from our Gaussian fits, the IRS 5 sources are extended.

>From our integrated flux densities at 1.3 and 0.7 cm, we have calculated spectral indices for sources IRS 5a, b, d1/d2, and f. Given the degree of blending, we now refer to d1 and d2 as d1/d2. Since the measurements were almost simultaneous, these results are not affected by variability. For IRS 5a, we find a negative index, which may indicate nonthermal emission. For the remaining three sources we derived positive spectral indices between 1.3 and 0.7 cm.

To calculate source parameters for sources IRS 5a, b, d1/d2, and f, we used our 1.3 cm data given in Table 1 and relationships in the Appendix. The results are presented in Table 4.

Although it is likely that some flux density variations have occurred, the data in Table 4 give us fairly reliable estimates. For these calculations, we have assumed an electron temperature of 10^4 K and uniform-density spherical sources. For deconvolved sizes less than half of the FWHP beam, we used $0.5\times$ the beamsize. Sources in our data are barely resolved, so the formulae in Mezger & Henderson (1967) were replaced by those in Panagia & Walmsley (1978). The use of the relations of Panagia & Walmsley (1978) means that we have radii that are twice the values that one obtains by simply setting source diameters equal to deconvolved FWHPs. The emission measures are very large, and the masses of ionized gas small. This would indicate that all of these are very young objects. We have not assigned stars for IRS 5a and f since these sources have clearly changed position since 1989.

Given the lack of proper motion, and the coincidence with IR sources (see Fig. 3), we find it likely that IRS 5d1/d2 and IRS 5b are ionized by internal OB stars. We classify the exciting stars of these regions by assuming that the Lyman continuum photons are not absorbed by dust and that the 1.3 cm emission is optically thin. If so, these regions are excited by early B stars. However the positive spectral indicies of the IRS 5d1/d2 and IRS 5b regions suggest that at least a part of the emission from these HCHII regions is optically thick. The strongest case can be made for IRS 5d1/d2. If the 1.3 cm flux density is due to optically thick free-free emission, but the 0.7 cm emission is optically thin, the Emission Measure will be a factor of 4, and an rms electron density a factor of 2 larger than the values in Table 4. It is possible that at 0.7 cm this nebula may still have a large free-free optical depth; such appears to be the case for the HCHII regions in W49 which show a continuous rising power law spectrum from 1.3 cm to 3 mm (Depree et al. (2001)). If IRS 5d1/d2 has optically thick free-free emission even to 3 mm and we extrapolate the 3 mm flux density using the measured spectral index, then the Emission Measure and rms electron density could be a factor of 15 and 4, respectively, larger than the values in Table 4.

IRS 5d1/d2 is the source with the largest increase in flux density, 2.3 mJy, between 1.3 and 0.7 cm (see Table 1). It is unlikely that the increase in flux density between 1.3 and 0.7 cm is caused by thermal dust radiation for several reasons. First, the spectral index is too small for dust emission, although this could be a mixture of free-free and dust radiation. Second, from equation 7 in the Appendix, we can determine the column density of protons, N(H). In a $0.2''$ beam, for a flux density of 3 mJy and dust temperature of 500 K, we have N(H)=5×10^{26} cm^{-2}. This is an extraordinary value; this column density must give rise to an extinction of greater than 10^4 visual magnitudes, so one needs a very special geometry to detect IRS 5d1/d2 even in the infrared. In the same fashion, assuming that the smaller increase in flux density found for IRS 5b is caused by dust emission and applying the same analysis, we find that the resulting extinction would be greater than 10^3 magnitudes. This is also an extremely large value; these HII regions are coincident with the 2μm. Hence it is unlikely that the positive spectral indicies determined for these HII regions are caused by thermal dust emission.

3.3. *Comparison with Near IR Data for W3*

We have overlayed the positions of our VLA sources on a NICMOS 2.22 μ meter image from the *HST* archive in Figure 3. This image was produced using the CALNICA V3.1.1 pipeline. The data, taken in the F222M filter, clearly resolve the infrared double source first reported by Howell, McCarthy & Low (1981). For IRS 5d1/d2 and IRS 5b, we find an excellent agreement between the R.A. and Declination arclengths measured from the NICMOS data and the VLA data. The two pairs of arclengths differ by only $0.007''$ and $0.002''$ in R.A. and Declination, respectively. These differences are within the errors of the VLA positions.

The difference in the absolute positions derived from the VLA and NICMOS data is $0.4''$ in Declination, which is within the expected uncertainties in the absolute pointing of NICMOS. After refining the absolute pointing of the NICMOS data using this offset, we find no sources at the positions of IRS 5a or IRS 5f in the NICMOS image. To corroborate the refinement of the NICMOS astrometry using the VLA data, we compared the refined NICMOS coordinates for an optically visible star with coordinates listed in the USNO A2 and B catalogs. We find offsets (R.A., Dec.) between our NICMOS position and those of the USNO A2 and B catalogs of (-0.20$''$, 0.03$''$) and (0.40$''$, -0.22$''$) respectively. The USNO positions from the two catalogs differ by (-0.60$''$, 0.25$''$), bracketing the NICMOS positions. Hence, we find a reasonable correspondence between the refined NICMOS positions and USNO catalog positions for this star. Given the excellent agreement between the relative offsets in the VLA and NICMOS data, we conclude that the near-IR double is spatially coincident with VLA sources IRS 5d1/d2 and IRS 5b.

3.4. *The Nature of IRS 5d1/d2 and IRS 5b*

These data provide a new insight into the nature of the radio sources and the relationship between the radio sources and infrared sources. The lack of proper motion between the radio sources IRS 5d1/d2 and IRS 5b, and the spatial coincidence found between the radio and near-IR positions shows that these trace ionized gas close to young OB stars. In contrast, the sources IRS 5a and f show significant proper motions in different directions, suggesting that these trace ionized gas in outflows driven by the embedded O–B stars ionizing IRS 5d1/d2 and IRS 5b.

The deconvolved angular radii of the IRS 5d1/d2 and IRS 5b radio sources are less than 240 AU. This is a generous limit based on spherical source geometry. It is only 1.3 times the radius at which the escape velocity for a $10M_\odot$ star is equal to 10 km s^{-1}, the sound velocity of the ionized gas. Thus it is possible that the ionized gas in IRS 5d1/d2 and IRS 5b is gravitationally bound to their exciting stars. The radius at which the escape velocity equals the thermal velocity is a critical point for both accretion flows in HII regions (Keto 2002) and stellar winds (Parker 1958); at this radius the wind/accretion flow transitions from subsonic to supersonic velocities. It is possible that the HII region can be trapped by accretion when the size of the Strömgren sphere is within this critical radius (Keto 2002). In both the accretion and wind models, the density of ionized gas rises toward the star, resulting in strongly peaked radio emission. The small size scales may also be indicative of photoevaporating disks (Hollenbach et al. 1994), in which the size of the optically thick HII region is on the order of 200 AU at 1.3 cm for an O7 star, assuming a weak stellar wind.

It is impossible at the moment to distinguish between these models. A feature of each of these models is a decreasing ionized gas density with radius, which can result in an increase of flux density with frequency (i.e. positive spectral indices) if

the cores of the HII regions are optically thick at the observed frequencies. Hence, these models can qualitatively explain the increase in flux seen between the 1.3 and 0.7 cm flux densities, although detailed modeling is needed to explore the stellar and gas properties required to reproduce the observed flux densities. A large optical depth is attractive given the mismatch between the high total infrared luminosity of IRS 5 (10^5 $L_\odot$; Campbell et al. 1995) indicating the presence of an O7 or O6 star, and the ionized gas parameters from the 1.3 cm data, which are consistent with B1-B0 stars. In this case, IRS 5d1/d2 with its large positive spectral index may be the more massive of the two sources, which is consistent with this source having both higher radio and 2 μm flux densities than IRS 5b.

Although we cannot currently distinguish between wind and accretion models, the small size of these regions does demonstrate that models of hypercompact HII region such as IRS 5d1/d2 and IRS 5b must include the influence of gravity from the exciting stars. In this way, models of hypercompact regions may differ significantly from models of ultracompact HII regions.

It is likely that the system is currently bound by the combined mass of the molecular gas and the two young stars, although it is not clear whether these will remain bound once the gas is dispersed. At the projected separation, the orbital velocity of a bound system would be $3-5$ km s^{-1}, assuming masses of 10 $M_\odot$ for IRS 5b and 10–50 $M_\odot$ for IRS 5d1/d2. In comparison, the full width at half maximum velocity measured in NH_3 observations with a $\sim 3''$ beam, which provides a reasonable upper limit to the relative velocities of the embedded stars, is 6 kms^{-1} ((Tieftrunk, Gaume & Wilson 1998)). This is slightly larger than the required orbital velocity.

3.5. *Nature of IRS 5a and IRS 5f*

Perhaps the best studied example of radio continuum sources in an outflow are the radio jets associated with the HH 80-81/GGD 27 complex (Marti, Rodriguez & Reipurth (1998), Marti, Rodriguez & Reipurth (1995)). The driving source is IRAS 18162-2048, with a luminosity of 2×10^4 $L_\odot$. Symmetrically distributed in a line about IRAS 18162-2048 are seven radio continuum knots. >From proper motions, these have velocities ranging from 500 to 1300 km s^{-1}, away from IRAS 18162-2048. There is a smooth decay of the free-free emission intensity with time for the two innermost components. In contrast, toward W3 IRS 5 we find no evidence for the symmetric, ordered motions apparent in HH 80-81. Although d1/d2 lies between the two radio sources with proper motions, IRS 5f and IRS 5a, source IRS 5a shows proper motions of a similar magnitude but in a roughly similar direction. If IRS 5d1/d2 is the *only* source driving the outflow, the motion of IRS 5a is difficult to explain, since one would expect source IRS 5a to be moving in the *opposite* direction. It is possible that there is a second outflow source, which may be IRS 5b. Imai et al. (2000) had reported two outflow centers. However, our second outflow center must be south of the position of IRS 5a, so this center must have a different location from the second water maser outflow source, which is north of IRS 5a. See our superposition of radio continuum sources, H_2O masers and near IR sources in Fig. 3. The lack of proper motion of continuum sources south of IRS 5d1/d2 and IRS 5b may result from an asymmetry in the surrounding dense molecular gas. There is also a distinct absence of masers directly south of IRS 5b (Imai et al. (2000)), which could also be explained by a lack of dense gas.

IRS 5a and f may be the result of either high-speed outflows, impinging on neutral dense clouds or ionized material ejected from the outflow sources. For electron densities of 10^5 cm^{-3}, the recombination time is on the order of years, and is shorter than the 36 year travel time estimated for IRS 5f. However, Marti, Rodriguez & Reipurth (1998) have shown that the moving sources in the HH 80-81/GGD 27 complex can be fitted with a model in which the free-free emission decays on a long timescale, and it is plausable that IRS 5a and IRS 5f are ionized globules undergoing a similar decay. Draine & McKee (1993) have reviewed interstellar shock phenomena. Dopita & Sutherland (1996) and Ghavamian & Hartigan (1998) have carried out simulations of fast shocks. The results show that a hundred km s^{-1} outflow can ionize neutral hydrogen. It is likely that the geometry of the outflows in W3 IRS 5 are conical regions in a northeast–southwest direction. The interior of this cone would be filled with low density gas. One can surmise that the CO outflow and H_2O masers are located toward the edges of this cone. More energetic phenomena involving ionized gas, such as IRS 5f and IRS 5a are found closer to the axis of cone, where the velocities are larger. In support of this picture, we find that the proper motions of the radio continuum sources are more than a factor of 2 larger than those measured for the H_2O masers. The molecular material studied by Helmich & van Dishoeck (1997) is easily dissociated, so must be farther from the high speed outflow. This may be located in disks associated with but perpendicular to the outflows.

4. CONCLUSIONS

On the basis of the analysis of our observations of the W3 IRS 5 hypercompact H II (HCHII) regions at 1.3 and 0.7 cm and comparisons with previous data from CG94 and TGC97, we conclude the following:

1. W3 IRS 5 sources d1/d2 and b exhibited no motion relative to one another to within $\sim$20 mas over the time period 1989.1 to 2002.5. We use these as a reference to investigate possible motions of sources IRS 5a and f.

2. The HCHII region IRS 5f is offset from the CG94 1989.1 position by $\sim$210 mas at a position angle of 12° east of north. This translates to a proper motion of 15.6 mas yr^{-1}, or a speed of 135 km s^{-1}.

3. IRS 5a is offset from the CG94 1989.1 position by $\sim$190 mas at a position angle of 50° east of north. This translates to a proper motion of 14.1 mas yr^{-1}. At the assumed distance to W3 IRS 5, this is an apparent speed of 122 km s^{-1}.

4. Using archival NICMOS data, we identify IRS 5d1/d2 and IRS 5b with the near IR sources first found by Howell, McCarthy & Low (1981). Given their lack of proper motion and coincidence with near IR sources, we conclude that these HII regions contain embedded stars. Our VLA measurements give upper limits of 240 AU to the sizes of the HII regions. These sources may be ionized by early B or O stars; we have only lower limits to the Lyman continuum flux from our continuum data.

5. Given the high velocities of the IRS 5a and IRS-f regions and the lack of any infrared sources toward these regions, we propose that these two regions are formed in the outflows originating in the W3 IRS 5 system. These

two HII regions may consist of shock ionized gas, or may be ionized knots expelled from the massive stars in W3 IRS 5.

6. The proper motions of the IRS 5a and IRS 5f suggest the presence of two outflows. IRS 5d1/d2 may be the outflow source causing the proper motion of IRS 5f, while IRS 5b may be the outflow source responsible for IRS 5a. Two different driving sources were also inferred from H_2O maser proper motions measured Imai et al. (2000). However, a fit to the proper motions of the H_2O masers results in an outflow source that is 300 mas north of IRS 5a, which is inconsistent with the direction of our proper motion for IRS 5a.

7. Both of the sources containing stars, IRS 5d1/d2 and IRS 5b have positive spectral indices. It is unlikely that this is due to dust emission, and is likely the result of a centrally condensed HII region that is optically thick toward the center of the region. A centrally condensed HII region could result from a wind or accretion flow.

8. Of the two sources with significant proper motions, IRS 5f has a slightly positive spectral index, which is significantly different from optically thin free-free emission, while IRS 5a shows a negative spectral index. The negative spectral index may indicate a contribution of synchroton emission.

9. From previous data, the flux densities of the HCHII regions IRS 5d2, d1, e, f, and g are larger at 6 cm than at 2 cm. This is further evidence that at longer wavelengths there may be a contribution to the emission from synchrotron radiation.

10. There is significant evidence for time variability for the W3 IRS 5 continuum sources between 1989.1 and 2002.5; the case is strongest for sources IRS 5e and g.

5. ACKNOWLEDGEMENTS

We thank M. Corbin(STScI) for help with the reduction of the NICMOS data from the HST archive.

6. APPENDIX

To obtain the correct values for emission measure, EM, the temperature T must be corrected for beam dilution. This is related to the main beam temperature, $T_{MB} = 60 \times S(mJy)$, by

$$T = T_{MB} \left(\frac{\theta(\text{observed})}{\theta(\text{source})} \right)^2 \quad (1)$$

where θ(observed) is the apparent source size, in Table 1, and θ(source) is the deconvolved size. To obtain the deconvolved source size, we used the geometric mean source size, and the usual deconvolution formula,

$$\theta(\text{source})^2 = \theta(\text{observed})^2 - \theta(\text{beam})^2 \quad (2)$$

θ(source) is the Full Width Half Power (FWHP) deconvolved source size in arc seconds. From Panagia & Walmsley (1978), for sources smaller than the beam, the conversion from Gaussian source FWHP to a spherical source radius is $\theta(\text{spherical source}) = 0.9 \times \theta(\text{source})$ To convert a size in arc seconds to a linear radius in parsecs for a distance of 1.83 kpc, we used $R(\text{spherical source}) = 0.008 \times \theta(\text{spherical source})$. For free-free radiation from ionized gas,

$$T = T_e \, (1 - e^{\tau_\nu}). \quad (3)$$

Assuming that $\tau \ll 1$, one can use the following expression for τ_ν to obtain the Emission Measure, EM, and RMS electron density, n_e

$$\tau_\nu = 8.235 \times 10^{-2} \left(\frac{T_e}{K} \right)^{-1.35} \left(\frac{\nu}{GHz} \right)^{-2.1} \left(\frac{EM}{pc \ cm^{-6}} \right) a(\nu, T). \quad (4)$$

For $T_e=10^4$ and ν=22.485 GHz, we have $EM = 2.13 \times 10^5 T$. The correction $\alpha(\nu, T)$ is usually $\cong 1$. If τ_ν is small compared to unity, then the rms electron density, n_e is given by:

$$n_e = 2.46 \left(\frac{T}{K} \right)^{0.5} \left(\frac{T_e}{K} \right)^{0.175} \left(\frac{\nu}{GHz} \right)^{1.05} \left(\frac{R}{pc} \right)^{-0.5}. \quad (5)$$

For $T_e=10^4$ and ν=22.485 GHz, we obtain

$$n_e = 324 \left(\frac{T}{K} \right) \left(\frac{R}{pc} \right)^{-0.5}$$

To calculate the mass of ionized gas we remove the extra electrons contributed by helium, whose abundance is y_n. Then the mass is given by:

$$\left(\frac{M}{M_\odot} \right) = 0.10 [1 + y_m] \left(\frac{R}{pc} \right)^3 \left(\frac{n_e}{cm^3} \right), \quad (6)$$

where y_m is the mass fraction of helium; for y_n=0.1, y_m=0.4. These calculations are for uniform density spheres. If there are gradients or clumps, the value of n_e is a lower limit and the mass is an upper limit to actual values.

For thermal emission from small dust particles, if the radiation is expressed in mJy, the source size, θ in arc seconds, peak flux density S_ν in mJy, and wavelength, λ in mm, the column density of hydrogen in all forms, N_H, in the Rayleigh-Jeans approximation, is given by the following relation (see Rohlfs & Wilson 1999):

$$N_H = 1.93 \times 10^{24} \left(\frac{S_\nu}{mJy} \right) \left(\frac{\theta}{''} \right)^{-2} \left(\frac{\lambda}{mm} \right)^4 \left(\frac{Z}{Z_\odot} \right)^{-1} \left(\frac{1}{b} \right) \left(\frac{T_{dust}}{K} \right)^{-1}. \quad (7)$$

In the centimeter and millimeter wavelength range, the dust optical depth usually increases with λ^{-2}; then flux density increases as λ^{-4}. If we take the metal abundance to be solar, $Z=Z_\odot$, the dust properties appropriate for a very dense gas, b=5 (see Ossenkopf & Henning 1994), $T_{dust}=5 \times 10^2$ K, λ = 7mm and $\theta = 0.2''$, we have $N(H) = 4.6 \times 10^{25} S_\nu$

REFERENCES

Campbell, M. F., Butner, H. M., Harvey, P. M., Evans, N. J. II, Campbell, M. B., & Sarbey, C. N. 1995, ApJ454, 831
Carilli, C. L. & Holdaway, M. A. 1997, VLA Scientific Memo, 173, 1
Claussen, M. J, Gaume, R. A., Johnston, K. J. & Wilson, T. L. 1994, ApJ, 424, L41
Claussen, M. J et al. 1984, ApJ, 285, L79
Colley, D., 1980, MNRAS 193, 495

DePree, C. G., Wilner, D. J., Goss, W.M. & Welch, W. J. 2001, BAAS, 33, 1502
Dopita, M. & Sutherland, R.S. 1996, ApJS, 102, 161
Draine, B.T. & McKee, C.F. 1993, ARA&A, 31, 373
Felli, M., Taylor, G.B., Catarzi, M., Churchwell, & Kurtz, S. 1993, A&AS, 101, 127
Gaume, R. A., Goss, W. M., Dickel, H. R. & Wilson, T. L. 1995, ApJ, 438, 776
Ghavamian, Parviz & Hartigan, Patrick 1998, ApJ501, 687
Helmich, F.P. & van Dishoeck, E.F. 1997, A&A124, 205
Hofner, P., Delgado, H., Whitney, B., Churchwell, E., & Linz, H. 2002, ApJ, 579, L95
Hollenbach, D. J., Johnstone, D., Lizano, S. & Shu, F. 1994 ApJ, 428, 654
Hollenbach, D. J. & Tielens, A. G. G. M. 1999 Rev. Mod. Phys., 71, 173
Howell, R. R, McCarthy, D. W. & Low, F. J. 1981, ApJ, 251, L21
Imai, H., Deguchi, S., Sasao, T. 2002, ApJ, 567, 971
Imai, H., Kameya, O., Sasao, T., Miyoshi, M., Deguchi, S., Horiuchi, S. & Asaki, Y. 2000, ApJ, 538, 751
Keto, E. 2002, ApJ, 580, 980
Ladd, E.F., Deane, J.R., Sanders, D.B. & Wynn-Williams, C.G. 1993, ApJ419, 186
Marti, J., Rodriguez, L.F. & Reipurth, B. 1998 ApJ, 502, 337
Marti, J., Rodriguez, L.F. & Reipurth, B. 1995 ApJ, 449, 184
Megeath, S. T., Herter, T., Beichman, C., Gautier, N., Hester, J. J., Rayner, J. & Shupe, D. 1996, A&A, 307, 775
Mezger, P.G. & Henderson, A.P. 1967, ApJ, 147, 471
Mitchell, G.F., Maillard, J.P. & Hasegawa, T.I. 1991, A&A, 371, 342
Neugebauer, G.; Becklin, E. E.; Matthews, K. 1982, AJ, 87, 395
Oldham, P.G., Griffin, M.J., Richardson, K.J. & Sandell, G. 1994, A&A, 284, 559
Ossenkopf & Henning, T. 1994, A&A, 291, 943
Parker, E. 1958, ApJ, 128, 664
Panagia, N. & Walmsley, M. 1978, A&A, 70, 411
Reid, M., Argon, A., Masson, C.R., Menten, K.M. & Moran, J.M. 1995, ApJ, 443, 238
Rohlfs, K. & Wilson, T.L. 1999, Tools of Radio Astronomy, 3rd edition, Springer-Verlag, Heidelberg
Roberts, D.A., Crutcher, R.M., Troland, T.H. & Goss, W.M. 1993, ApJ, 412, 675
Schleuning, D.A., Vaillancourt, J.E., Hildebrand, R.H., Dowell, C.D., Novak, G., Dotson, J.L. & Davidson, J.A. 2000, ApJ, 535, 913
Tieftrunk, A. R., Gaume, R. A. & Wilson, T. L. 1998, A&A, 340, 242
Tieftrunk, A. R., Gaume, R. A., Claussen, M. J., Wilson, T. L. & Johnston, K. J. 1997, A&A, 318, 931
Tieftrunk, A. R., Wilson, T. L., Steppe, H., Gaume, R. A., Johnston, K. J. & Claussen, M. J. 1995, A&A, 303, 901
Wilner, D. J., Reid, M. J., & Menten, K. M. 1999, ApJ, 513, 775
Wynn-Williams, C. G., Becklin, E. E., & Neugebauer, G. 1972, MNRAS, 160, 1

TABLE 1

GAUSSIAN FITS TO THE 1.3 AND 0.7 CM DATA.

W3 IRS 5 Source	λ (cm)	α (B1950) $2^h\ 21^m$	δ (B1950) $61^\circ\ 52'$	Major Axis ($''$)	Minor Axis ($''$)	Position[a] Angle ($^\circ$)	Flux Density Peak (mJy/beam)	Flux Density Integrated (mJy)
a	1.3	53.2196±0.0025[s]	20.939±0.036$''$	0.399±0.084	0.196±0.041	1.30±11.01	0.654±0.014	1.279±0.036
b	1.3	53.2250±0.0009[s]	20.515±0.009$''$	0.295±0.020	0.208±0.014	1.11±7.65	2.055±0.014	3.158±0.033
d1/d2 ...	1.3	53.3248±0.0003[s]	21.514±0.003$''$	0.263±0.006	0.193±0.004	11.66±3.01	6.169±0.014	7.816±0.029
f	1.3	53.4044±0.0009[s]	22.491±0.007$''$	0.240±0.017	0.209±0.015	4.53±21.33	2.013±0.014	2.523±0.029
a	0.7	53.2204±0.0016[s]	20.977±0.015$''$	0.215±0.037	0.156±0.027	11.74±21.23	0.967±0.016	0.814±0.025
b	0.7	53.2236±0.0005[s]	20.492±0.005$''$	0.239±0.012	0.187±0.009	0.23±7.84	3.398±0.016	3.804±0.031
d1/d2 ...	0.7	53.3260±0.0002[s]	21.495±0.002$''$	0.251±0.005	0.194±0.004	17.29±3.04	8.339±0.016	10.151±0.032
f	0.7	53.4044±0.0010[s]	22.484±0.008$''$	0.256±0.020	0.206±0.016	168.81±14.59	2.070±0.016	2.734±0.034

[a] The uncertainty quoted was obtained from gaussian fits to the images. To obtain agreement with the maxima IRS 5d1/d2 and b from CGJW, a shift of $\sim$20 mas in $\alpha\cos(\delta)$ was needed. This may be the size of the systematic positional error.

TABLE 2

ARCLENGTH DIFFERENCES BETWEEN OUR DATA AND CGJW.

Arclength[a]	λ cm	Δ R.A. ($''$)	Δ Dec. ($''$)	Total Offset ($''$)	Position Angle[b] ($^\circ$)
f-d1/d2 ..	0.7	0.045	0.209	0.214	12.2
d1/d2–b .	0.7	0.002	0.013	0.013	10.2
f–b	0.7	0.047	0.221	0.227	12.1
a-d1/d2 ..	0.7	0.123	0.143	0.188	40.7
a–b	0.7	0.125	0.155	0.200	38.9
f–d2	1.3	0.054	0.196	0.204	15.3
d1/d2–b .	1.3	-0.016	0.009	0.019	120.5
f–b	1.3	0.038	0.206	0.209	10.4
a-d1/d2 ..	1.3	0.126	0.085	0.152	56.0
a–b	1.3	0.110	0.094	0.145	49.3

[a]Designates arclength between two respective W3 IRS 5 source components for which we measured differences between our data and that of CGJW.

[b]Position angle measured East of North.

TABLE 3

COMPARISON OF W3 IRS 5 SOURCE FLUX DENSITIES

W3 IRS 5 Source	Total Flux Density (mJy) 6cm	2cm	1.3cm	0.7cm
a	0.6[d]	0.6[d]; 0.52[c]	0.3[d]; 1.3[a]	0.8[a]
b	0.8[d]	0.7[d]; 0.78[c]	0.6[d]; 3.2[a]	3.8[a]
a+b	...	...	2.0[c]	...
c	0.7[d]	0.6[d]; 0.56[c]	<0.3[d]; <0.45[b]	<0.48[b]
d1.....	1.7[d]	0.8[d]; 0.48[c]	1.9[d]; <1.5[b]	<2.1[b]
d2	2.6[d]	1.8[d]; 1.02[c]	4.2[d]; 7.8[a,e]	10.2[a,e]
c+d	...	...	2.5[c]	...
e	2.0[d]	1.0[d]; 0.36[c]	0.7[d]; <0.45[b]	<0.48[b]
f	1.8[d]	0.6[d]; 0.72[c]	0.8[d]; 2.5[a]	2.7[a]
e+f	...	...	1.4[c]	...
g	0.5[d]	0.3[d]; ... [c]	0.6[d]; <0.45[b]	<0.48[b]

[a]From Gaussian fit to image peak.

[b]Estimate from task IMEAN (see text).

[c]Data from CGJW.

[d]Data from TGCWJ.

[e]Possible contamination from d1.

TABLE 4
PARAMETERS OF THE IONIZED REGIONS

W3 IRS 5 Source	Spectral Index	Peak Flux Density (mJy/beam)	Angular[a] Size ($''$)	Peak[b] Temp. (K)	Emission Measure ($cm^{-6}pc$)	Radius (pc)	Electron[c] Density (cm^{-3})	Mass[c] ($M_\odot$)	Spectral[d] Type
a	-0.69±0.06	0.6	0.28	80	1.7(7)	1.6(-3)	7.3(4)	3.5(-5)	... [e]
b	0.28±0.02	2.0	0.25	340	7.2(7)	1.2(-3)	1.7(5)	3.8(-5)	B0.5- B1
d1/d2 ...	0.39±0.01	6.2	0.22	1800	3.7(8)	8.0(-4)	4.8(5)	3.1(-5)	B0.5- B1
f	0.12±0.02	2.0	0.22	580	1.2(8)	8.0(-4)	2.8(5)	1.8(-5)	... [e]

[a]Geometric mean of angular sizes in Table 1.

[b]Corrected for beam dilution; if deconvolved size $< 0.1''$, we used $0.1''$. see Appendix.

[c]see Appendix.

[d]see Rohlfs & Wilson 1999

[e]These are sources with proper motions; see text for details.

Figure Captions

FIG. 1.— Continuum image of the W3 IRS 5 region at 1.3 cm (Epoch 2002.5). The FWHM beam size is $0.2'' \times 0.2''$. Contour levels are -1, 1, 2, 4 and 8 times the 3σ RMS noise in the image of 0.45 mJy/beam. The peak flux density is 6.16 mJy/beam, which corresponds to a main beam brightness temperature of 371.8 K. The crosses designate positions of sources IRS 5a, b, c, d1, d2, e, and f from CGJW and the position of source IRS 5g from TGCWJ (Epoch 1989.1). In our beam, IRS 5d1 and d2 are blended.

FIG. 2.— Continuum image of the W3 IRS 5 region at 0.7 cm (Epoch 2002.5). The FWHM beam size is $0.2'' \times 0.2''$. Contour levels are -1, 1, 2, 4, 8 and 16 times the 3σ RMS noise in the image of 0.48 mJy/beam. The peak flux density is 8.34 mJy/beam, which corresponds to a main beam brightness temperature of 135 K. The crosses designate positions of sources IRS 5a, b, c, d1, d2, e, and f from CGJW and the position of source IRS 5g from TGCWJ (Epoch 1989.1). In our beam, IRS 5d1 and d2 are blended.

FIG. 3.— NICMOS 2.22 μm image of the W3-IRS 5 region. The greyscale image shows the near-IR double, with the positions of IRS 5d1/d2 and IRS 5b marked. The orientation of the data is B1950, the offsets are relative to the position of IRS 5d1/d2, A previously undetected source is apparent in the NICMOS image between IRS 5d1/d2 and IRS 5b; this source appears extended. The positions of sources IRS 5a and IRS 5f are marked with arrows showing the direction and magnitude of the proper motions between Epochs 1989.1 and 2002.5. Also shown are the positions of the H_2O masers (Imai et al. 2000). The lengths and directions of the arrows show the expected proper motions of the masers over a 100 year period relative to an arbitrary inertial reference center. Note that the maser motions are shown over a 100 year period while the continuum source motions are shown over a 13 year period. The proper motions of the continuum sources are typically a factor of 2 more larger than than those of the masers.

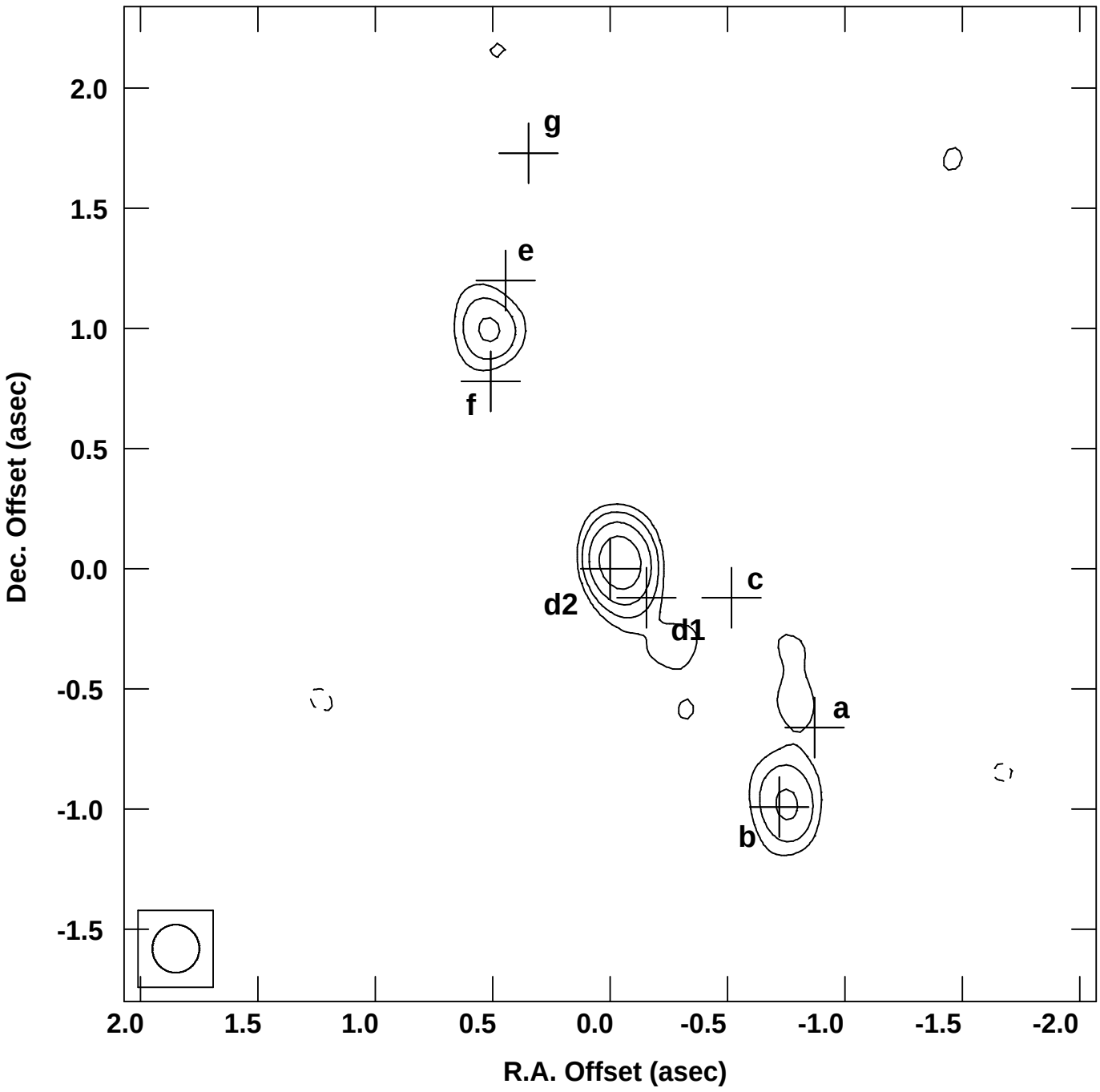
g
e
f
d2
d1
c
a
b
2.0
1.5
1.0
0.5
0.0
-0.5
-1.0
-1.5
-2.0
Dec. Offset (asec)
R.A. Offset (asec)

Figure 1

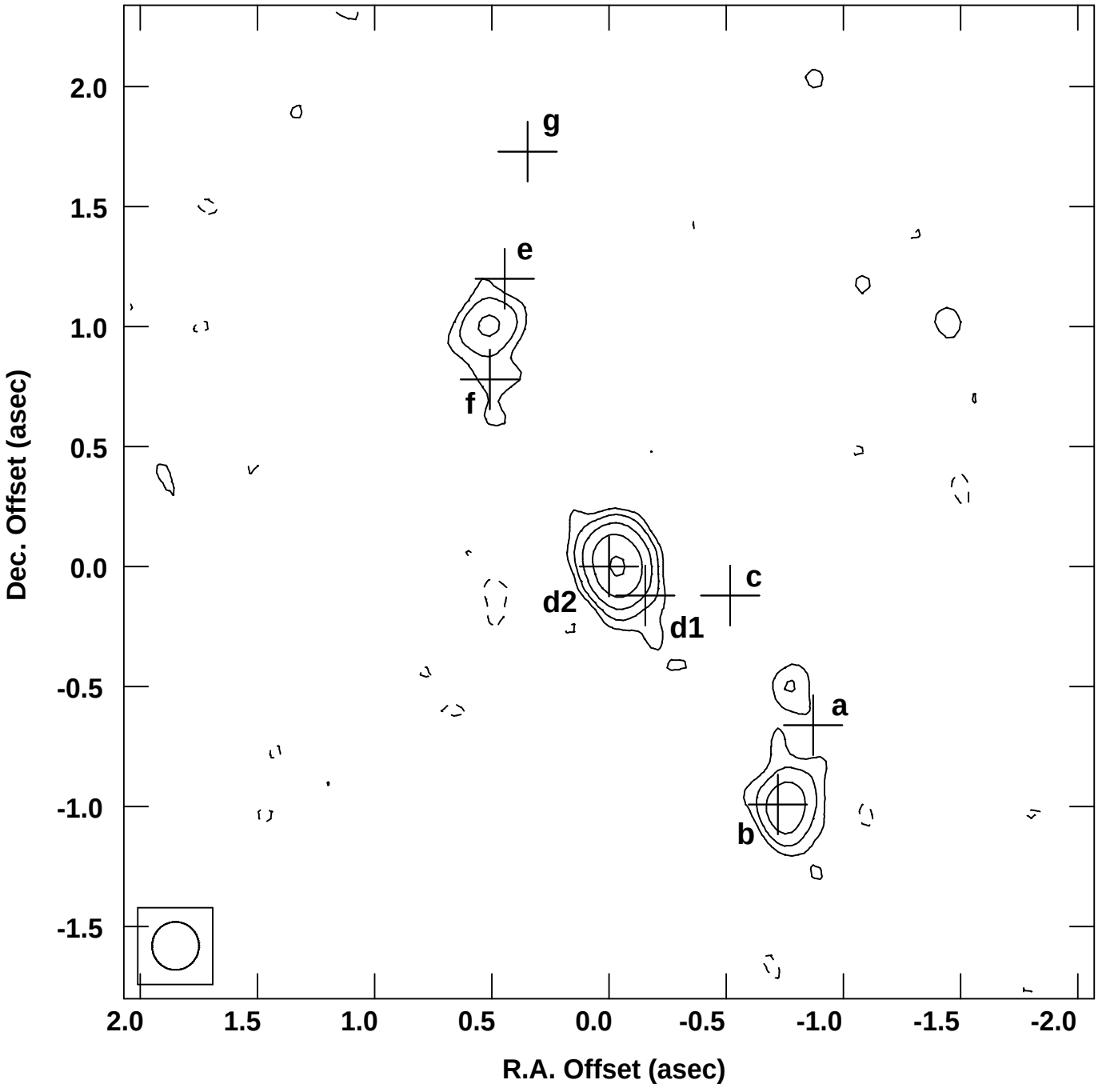
g
e
f
d2
d1
c
a
b
2.0
1.5
1.0
0.5
0.0
-0.5
-1.0
-1.5
-2.0
Dec. Offset (asec)
R.A. Offset (asec)

Figure 2

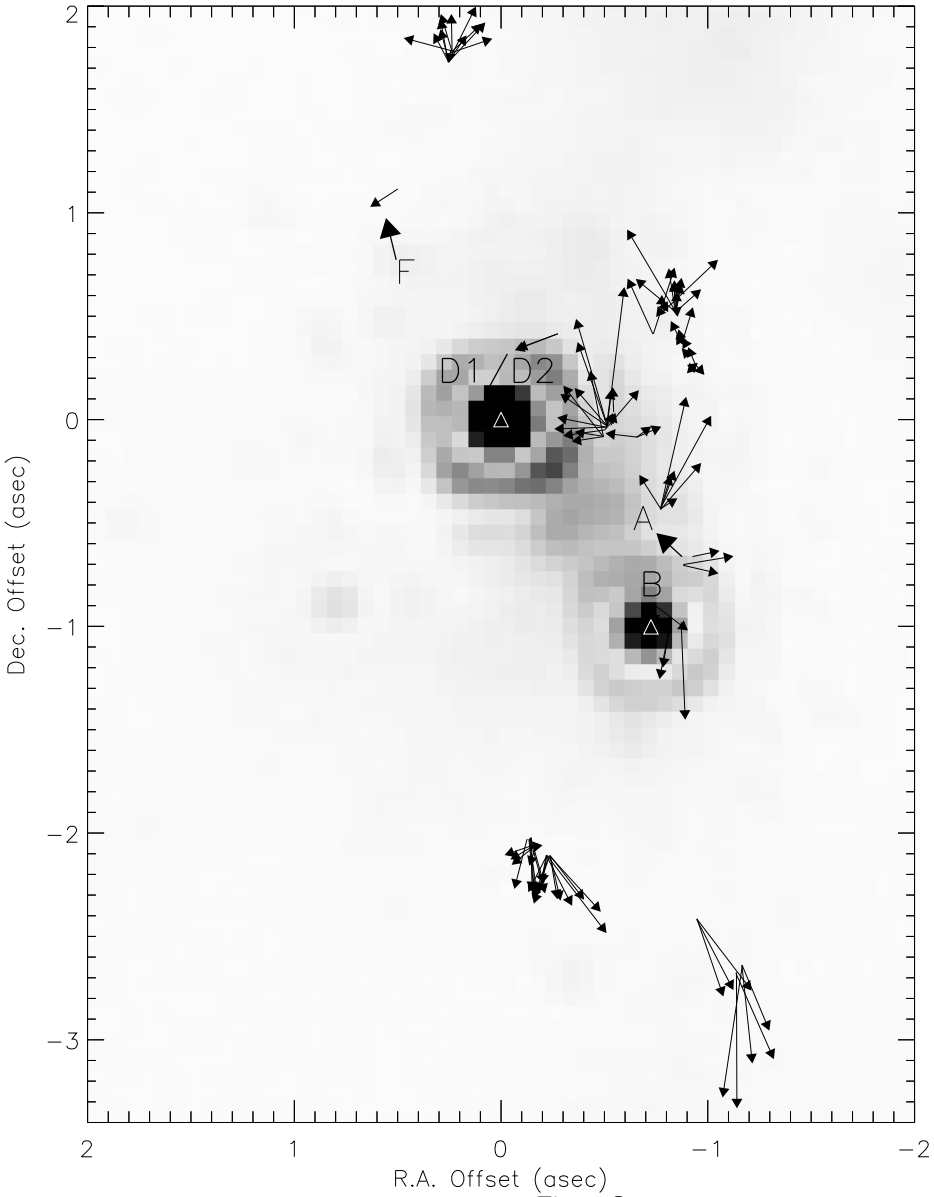

Figure 3